Composites Communications 37 (2023) 101429

Contents lists available at ScienceDirect

Composites Communications

journal homepage: www.elsevier.com/locate/coco

Hierarchically porous polyimide aerogel fibers based on the confinement of $Ti_3C_2T_x$ flakes for thermal insulation and fire retardancy

Dan Wang [a], Yidong Peng [a], Jiancheng Dong [a], Lei Pu [a], Kangqi Chang [a], Xiu-Ping Yan [b], Hai-Long Qian [b], Le Li [a,**], Yunpeng Huang [a,*], Tianxi Liu [a,***]

[a] Key Laboratory of Synthetic and Biological Colloids, Ministry of Education, School of Chemical and Material Engineering, Jiangnan University, Wuxi, 214122, China
[b] School of Food Science and Technology, Jiangnan University, Wuxi, 214122, China

ARTICLE INFO

Keywords:
Aerogel fibers
Multi-scale porosity
Liquid-solid phase separation
Thermal insulation
Flame resistance

ABSTRACT

Thermally insulating and flame-resistant fibers/textiles have drawn enormous attention attributing to their great application prospects in personal thermal management and protective clothing. Nevertheless, conventional natural fibers and synthetic fibers are insufficient for advanced thermal regulation. Herein, an in-situ polymerization method and wet-spinning technique are employed for the continuous and scalable fabrication of polyimide (PI) aerogel fibers utilizing monolayered $Ti_3C_2T_x$ flakes as the pore-generating agents. Benefiting from the intimate interfacial interaction between MXene and the macromolecular chains, hierarchical porosity is constructed in the composite aerogel fibers due to the confinement of the interconnected PAA/$Ti_3C_2T_x$ networks during liquid-solid phase separation. As a result, the PI/$Ti_3C_2T_x$ aerogel fibers manifest significantly enhanced mechanical properties (tensile strength of 26 MPa), large specific surface area (145 $m^2\ g^{-1}$), excellent flame resistance, and remarkable thermal insulation performance (with a low thermal conductivity of 36 mW $m^{-1}\ K^{-1}$), which can be readily weaved into flexible textiles for practical thermal regulating applications. This approach is expected to pave a new way for the fabrication and application of high-performance thermal insulating fibers and textiles.

1. Introduction

Human thermal comfort is not only of great significance to physical and mental health, life safety, and social production efficiency, but also greatly affects the energy consumption of building heating, ventilation, and air conditioning (HVAC) systems [1-3]. Moreover, infrared stealth in the military field is an important guarantee to increase the survivability of weapons on the battlefield, which has a wide range of applications in the areas of the individual soldier or UAV system [4-6]. As the medium between the ambient and human body, textiles play a vital role in heat conduction and insulation for personal thermal regulation. A variety of conventional fibers/textiles including natural fibers [7,8] (cotton fibers, wool fibers, silk fibers) and synthetic fibers [9,10] (such as polyester fibers, polyolefin fibers, polyamide fibers, polyacrylonitrile fibers et al.) have been fabricated to meet the various wearing acquirements of people, which can hardly satisfy the rigorous conditions for advanced thermal regulation. Therefore, developing new strategies and novel materials for high-performance thermal management is highly necessary and promising in both academic and industrial communities.

Recently, structure-engineered synthetic fibers with hollow morphology and ultrafine diameters were fabricated for improved thermal insulation. It is proved that the large surface area provided by the hollow interior and thinner fibers are highly beneficial for air trapping [11]. It is also reported that the thermal insulation performance of fibers is especially dependent on their density, porosity, and pore size [12]. Aerogel is one kind of porous bulk material featuring ultra-low density and high porosity, possessing wide applications in adsorbing material, energy storage electrodes, and heat-insulating materials [13-18]. Integrating the advantages of aerogels and fibers/textiles, the burgeoning aerogel fibers featuring excellent thermal and electrical conductivity, as well as high porosity, e.g., graphene aerogel fibers,

* Corresponding author.
** Corresponding author.
*** Corresponding author.
E-mail addresses: le_li@jiangnan.edu.cn (L. Li), hypjnu@jiangnan.edu.cn (Y. Huang), txliu@jiangnan.edu.cn (T. Liu).

https://doi.org/10.1016/j.coco.2022.101429
Received 17 September 2022; Received in revised form 18 November 2022; Accepted 20 November 2022
Available online 25 November 2022

silica and cellulose aerogel fibers, have demonstrated great potential in smart fabrics, acoustic applications, thermal insulation materials, etc. [19,20]. For example, Zhang and coworkers [21] reported a robust and flexible polyimide aerogel fiber through a sol-gel confined transition strategy, which manifested excellent thermal insulation performance due to the high surface area (up to 364 $m^2 g^{-1}$). Bai et al. [22] used a freeze-spinning technique to continuously fabricate silk aerogel fibers with porous structures mimicking the polar bear hair, the biomimetic fibers and woven showed excellent thermal insulation properties and good air permeability. Researchers also fill the fibers with thermal insulation materials to effectively reduce thermal conductivity by improving the scattering of phonons at the solid-solid and solid-gas interfaces [23,24]. However, previously reported aerogel fibers often suffer from a performance compromise between mechanical strength and thermal insulation properties.

Polyimide (PI) with excellent thermal insulation, low dielectric constant, and excellent mechanical properties possess great potential in the fabrication of high-performance polymeric aerogels [25-27]. In this work, we report the thermal insulating and flame-resistive PI/$Ti_3C_2T_x$ aerogel fibers through the continuous wet-spinning of in-situ polymerized polyamic acid (PAA)/$Ti_3C_2T_x$ composite solution. Taking advantage of the intimate interfacial interaction between $Ti_3C_2T_x$ flakes and the macromolecular chains, hierarchical porosity is engineered in the composite aerogel fibers due to the confinement of the interconnected PAA/$Ti_3C_2T_x$ networks during liquid-solid phase separation. Fabricated aerogel fibers not only possess multi-scale porosity and excellent mechanical properties, and also manifest desirable thermal insulation and flame-resistance performance. More importantly, obtained PI/$Ti_3C_2T_x$ aerogel threads can be readily weaved into thermo-regulating textiles for wearable applications. Considering the feasibility, scalability, and functionality of prepared PI aerogel fibers, this work can help the development of next-generation synthetic fibers and textiles for thermal management.

2. Experimental

2.1. Materials

4,4′-oxidianiline (ODA, 98%), *N,N*-dimethylacetamide (DMAc, 99.8%), and triethylamine (TEA, >99.5%) were obtained from Adamas Reagent Co., Ltd. Pyromellitic dianhydride (PMDA, ≥98.5%), 37 wt % hydrochloric acid (HCl), and ethyl alcohol (99.5%) were purchased from Sinopharm Chemical Reagent Co., Ltd. Ti_3AlC_2 (400 mesh) was supplied by Jilin 11 Technology Co., Ltd. Lithium fluoride (LiF, 99.995%) was bought from Aladdin Chemistry Co., Ltd, China.

2.2. In-situ polymerization of PAA/$Ti_3C_2T_x$

$Ti_3C_2T_x$ was synthesized using the minimally intensive layer delamination (MILD) method by etching the Al layer from Ti_3AlC_2 MAX powder. Briefly, 2 g LiF was dissolved in 40 mL 9 M HCl solution in a polytetrafluoroethylene container, followed by stirring for 30 min at room temperature. 2 g Ti_3AlC_2 powder was then slowly added to the above solution under magnetic stirring at 35 °C for 24 h. Obtained blackish sediment was washed several times under 3500 rpm centrifugation for 10 min until the pH reached approximately 6. The neutral $Ti_3C_2T_x$ sediment was then re-dispersed in ethyl alcohol under ultrasonication for 1 h to form the monolayered $Ti_3C_2T_x$ suspension. $Ti_3C_2T_x$ powder was finally produced by freeze-drying at −60 °C for 120 h.

PAA/$Ti_3C_2T_x$ solution was prepared via an in-situ polymerization technique. To start with, freshly synthesized $Ti_3C_2T_x$ powder was dispersed in 96 g DMAc under ultrasonication for 1 h to form the suspensions with different $Ti_3C_2T_x$ concentrations. Then, 8 g ODA was dissolved in the suspension, and 8.8 g PMDA was subsequently added to the solution and stirred in an ice bath for 3 h. Finally, 4 g TEA was dropwise added into the above mixture and stirred for 5 h. Obtained composite solutions were denoted as PAA/$Ti_3C_2T_x$-*x* (x = 2, 5, 10), in which x represents the weight percentage of the $Ti_3C_2T_x$ in the total weight of ODA and PMDA. For comparison, a neat PAA solution was also prepared without the addition of MXene.

2.3. Wet-spinning of PI/$Ti_3C_2T_x$ aerogel fibers

The freshly prepared PAA/$Ti_3C_2T_x$ solution was pumped into a DI water coagulation bath using a 23-gauge blunt-tip spinneret. The flow velocity was regulated using a syringe pump (1–3 mL min^{-1}). A homemade receiving roller driven by a gearmotor was utilized to collect the fibers, generated fibers were finally transferred into DI water to completely remove the residual solvent in PAA. The collecting speed of the roller was set at 1.5 mm s^{-1} to ensure optimized fiber uniformity and complete coagulation. Neat PAA fibers were also spun through the same procedure. The PAA/$Ti_3C_2T_x$ fibers and PAA fibers were eventually thermal imidized in an oven. To guarantee full imidization, the temperature was gradually raised at a rate of 2 °C min^{-1} and held at 100, 180, and 250 °C for 30, 30, and 120 min, respectively, before cooling.

2.4. Characterization

Morphologies of the fibers were observed by scanning electron microscopy (SEM, Hitachi, S4800). The cross-section surfaces were created by submerging the fiber in liquid nitrogen for 1 min and then fracturing it. The distribution of elements on the samples was scanned by EDS. The chemical structures of the samples were analyzed using a Fourier transform infrared spectroscopy (FTIR, Thermo Electron Corporation, Nicolet 6700). X-ray diffraction (XRD) patterns of the samples were collected on an AXS diffractometer (Bruker, D8) with Cu Kα generated at 40 kV and 40 mA at a scanning rate of 0.05° s^{-1} over a 2θ range of 5°–90°. The infrared thermal images were taken by a thermal imager (Fluke, Ti400+). Thermal conductivity was determined by a hot disk thermal analyzer (Hot Disk TPS 2500S, Sweden) based on the transient plane source method (ISO 22007-2:2015). Thermogravimetric analysis (TGA) was carried out on a DSC/TG synchronous thermal analyzer (Mettler Toledo, 1100SF). The mechanical properties of the fibers were measured using a tensile testing instrument (Suns, UTM2203) equipped with a 5 N load cell. The pore structure and pore size distribution of the samples were analyzed by the BJH nitrogen adsorption and desorption method (Quantachrome, Autosorb iQ2). The specific surface area of the samples was determined at 77 K by the BET method.

3. Results and discussion

Due to the high viscosity of polyimide (PI) and polyamic acid (PAA, percussor of PI), it is very difficult to realize the uniform dispersion of monolayered MXene in PAA and PI. Hence, an in-situ polymerization technique was employed in this work to prepare a homogeneous PAA/$Ti_3C_2T_x$ spinning solution by conducting PMDA/ODA polymerization in $Ti_3C_2T_x$/DMAc dispersion (Fig. 1(a)). To start with, $Ti_3C_2T_x$ flakes with single-/few-layered structure were successfully synthesized via mild etching and exfoliation. It can be seen from Fig. S1(a) that the freshly-synthesized MXene was evenly dispersed in DMAc with an obvious Tindal effect. Besides, the lateral dimension and thickness of the MXene flake characterized by AFM were approximately 2.0 μm and 2.8 nm, respectively, demonstrating the monolayered structure of the flakes (Fig. S1(b) and S1(c)). After that, PAA/$Ti_3C_2T_x$ solutions with different MXene mass fractions were prepared by controlling the MXene content in the DMAc solvent. As shown in Fig. S2, prepared PAA/$Ti_3C_2T_x$ solutions exhibit homogeneous greyish appearances, the viscosity of the composite solution decreases significantly with the increase of MXene fraction.

A homemade wet-spinning apparatus was then utilized to fabricate the PAA/$Ti_3C_2T_x$ fibers through a coagulation bath of DI water (Fig. 1(b) and S3). As presented in Video S1, the black fibers can be continuously

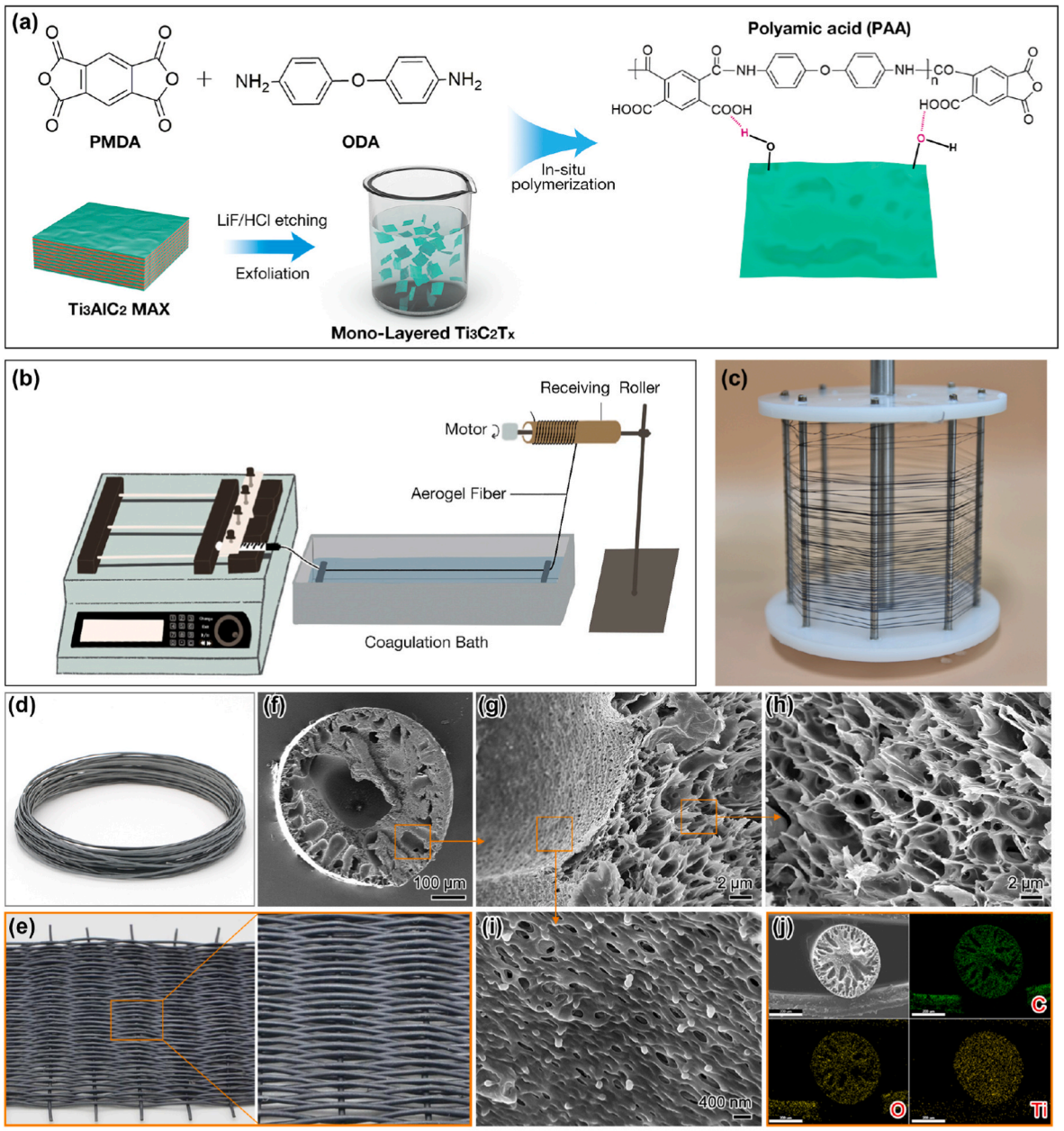

Fig. 1. (a) Schematic for the in-situ polymerization of PAA/$Ti_3C_2T_x$ spinning solution. (b) Illustration of the wet-spinning process. (c) Digital photograph of the freshly-prepared PAA/$Ti_3C_2T_x$-5 composite fibers. (d) Digital photographs of the PI/$Ti_3C_2T_x$-5 composite fibers, and (e) the weaved textiles. (f-i) Cross-sectional SEM images of the PI/$Ti_3C_2T_x$-5 aerogel fibers, and (j) corresponding elemental mapping.

generated through the orifice using the PAA/$Ti_3C_2T_x$ solutions, which were collected on a steel roller for further thermal imidization (Fig. 1(c)). Obtained PI/$Ti_3C_2T_x$-5 composite fibers manifested great shape uniformity and decent mechanical strength, which can be weaved to large-size PI/$Ti_3C_2T_x$ textile for further applications (Fig. 1(d) and (e)). SEM image in Fig. 1(f) reveals the circular cross-section of wet-spun PI/$Ti_3C_2T_x$-5 fibers, from which abundant pores and voids can be observed existing in the composite fiber. It is also interesting to find that the pore size decreased from the center to the edge (Fig. 1(f)), which may be ascribed to the gradual solvent exchange during the spinning process. More excitingly, hierarchical porous structures are verified by high-resolution SEM observation in Fig. 1(g)-1(i). It is demonstrated that the matrix of PAA/$Ti_3C_2T_x$ fiber is filled with honeycomb-like micro voids with a size of about 20 μm. Whereas, the wall of the macro pores presents a completely different stoma-like porosity with a mean diameter of about 2 μm. According to a previously reported work by Zhu et al., the hollow structure in the center of PI/$Ti_3C_2T_x$ aerogel fiber may be stemmed from the progressive diffusion of PAA outward with DMAc in the coagulating bath [28]. Further elemental mapping on the cross-section shows the uniform distribution of the Ti element, verifying the successful hybridization of MXene in the fiber (Fig. 1(j)).

Supplementary data related to this article can be found at https://doi.org/10.1016/j.coco.2022.101429.

The morphologies of pure PI, PI/$Ti_3C_2T_x$-2, and PI/$Ti_3C_2T_x$-10 fibers are also carefully characterized in Fig. 2(a)-2(l). The optical images indicate that the color of the fibers gradually deepened with increasing the weight percentage of $Ti_3C_2T_x$. Same as PI/$Ti_3C_2T_x$-5, all of these fibers present relatively uniform circular shapes and porous structures in the cross-section. As for the pores in the matrix and on the macro-pore walls, significant differences can be seen for the wet-spun fibers with varied MXene content. Specifically, apart from the macro pores in the cross-section, neat PI fibers show poor porosity with few voids in both

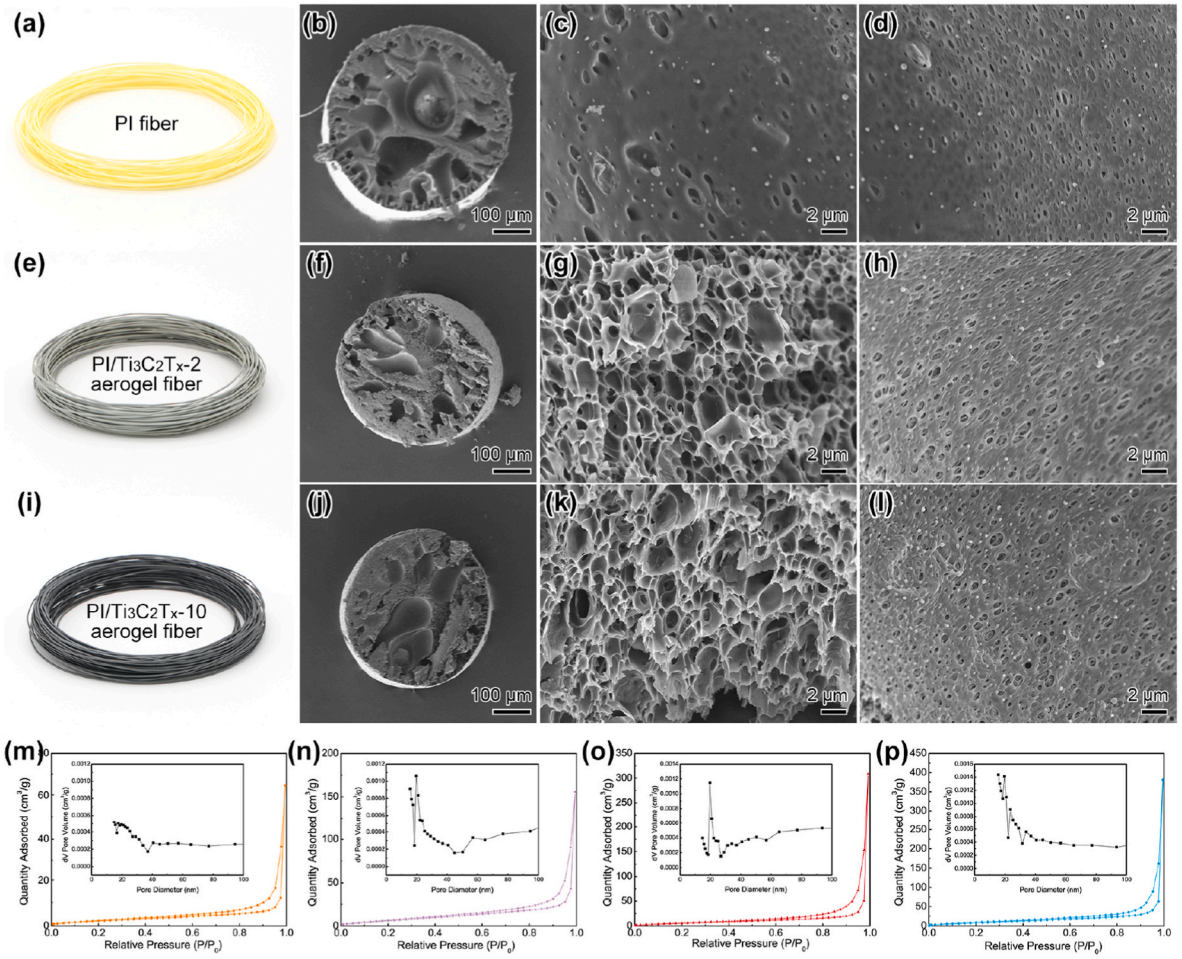

Fig. 2. Digital photographs and cross-sectional SEM images of different wet-spun fibers: (a-d) pure PI fiber, (e-h) PI/$Ti_3C_2T_x$-2 aerogel fiber, and (i-l) PI/$Ti_3C_2T_x$-10 aerogel fiber. N_2 adsorption-desorption curves and corresponding pore distributions: (m) pure PI fiber, (n) PI/$Ti_3C_2T_x$-2 aerogel fiber, (o) PI/$Ti_3C_2T_x$-5 aerogel fiber, and (p) PI/$Ti_3C_2T_x$-10 aerogel fiber.

regions. However, the above situation is largely improved after the addition of only 2 wt% MXene, the PI/$Ti_3C_2T_x$-2 composite fiber manifests well-defined porous morphologies both in the matrix and macropore walls. Further increase in the $Ti_3C_2T_x$ content yields the same hierarchical porous structure in PI/$Ti_3C_2T_x$-10, despite the significant decrease of the fiber diameter due to the lower viscosity of the PAA/$Ti_3C_2T_x$-10 solution. Finally, the specific surface areas and pore-size distributions of pure PI, PI/$Ti_3C_2T_x$-2, PI/$Ti_3C_2T_x$-5, and PI/$Ti_3C_2T_x$-10 fibers were studied using N_2 adsorption-desorption technique. As presented in Fig. 2(m)-2(p), the specific surface area of PI/$Ti_3C_2T_x$ aerogel fibers increases steadily with the MXene content from 16.7 $m^2\ g^{-1}$ (PI fiber), 42.3 $m^2\ g^{-1}$ (PI/$Ti_3C_2T_x$-2 fiber), 76.4 $m^2\ g^{-1}$ (PI/$Ti_3C_2T_x$-5 fiber), to 145 $m^2\ g^{-1}$ (PI/$Ti_3C_2T_x$-10 fiber). The above results indicate that the MXene flakes play a vital role in the formation of micro-pores in the aerogel fibers.

The structural features of the PI/$Ti_3C_2T_x$ aerogel fibers were systematically studied by XRD and FTIR. As displayed in Fig. 3(a), an amorphous diffraction peak at ~20° in the spectrum of PI is ascribed to the dehydration cyclization of the PAA precursor after imidization. $Ti_3C_2T_x$ exhibits a characteristic sharp peak located at about 6.3°, which appears in the spectrum of PI/$Ti_3C_2T_x$ and PI/$Ti_3C_2T_x$ but with significantly weakened peak intensity, indicating the crystalline structure of $Ti_3C_2T_x$ is influenced after hybridizing with PI. Fig. 3(b) displays the FTIR spectra of different samples. The absorption peaks of pure PAA at 1498 cm^{-1}, 1539 cm^{-1}, 1650 cm^{-1}, 3055 cm^{-1}, and 3261 cm^{-1} can be readily indexed to the C–N, C═C, C═O, -OH, and N–H groups on PAA chain. The N–H and -OH peaks disappear after thermal imidization under 300°C, confirming the successful imidization of PAA. After the in-situ polymerization of PAA in MXene dispersion and subsequent thermal treatment, most of the absorption peaks disappear significantly, while the peaks of C═O, C–N, and C═C shift to lower wavenumbers, which can be attributed to the strong hydrogen bonding between the = O/-NH groups on PI and the -OH groups on $Ti_3C_2T_x$ flakes (Fig. 3(c)). The possible pore-forming mechanism is schematically illustrated in Fig. 3 (d). It is speculated that MXene flakes can form intimate bonding with PAA chains through the strong hydrogen bonding between the amino groups on PAA and the hydroxyl groups on MXene, resulting in the evenly distributed interconnected MXene networks in the PAA matrix. During the coagulation process in a water bath, the diffusion of DMAc molecules will be restricted in limited spaces due to the confinement of PAA/$Ti_3C_2T_x$ networks, thus leading to the liquid-solid phase separation in the composite fibers, and finally giving birth to the hierarchical porosity after removal of DMAc after heat treatment.

To investigate the thermal stability of the PI/$Ti_3C_2T_x$ aerogel fibers, TGA was performed in nitrogen at a heating rate of 20 °C min^{-1}. As shown in Fig. 3(e), the thermal decomposition process of the above materials can be divided into two steps, the slight weight decrease caused by the evaporation of adsorbed water and the decomposition of surface groups at around 300 °C, and massive weight loss at 525°C–625°C due to the thermal decomposition of polyimide. The weight loss of $Ti_3C_2T_x$ mainly comes from its dehydration reaction Ti–OH + Ti–OH→H_2O + Ti–*O*–Ti [29]. Besides, the PI/$Ti_3C_2T_x$-10

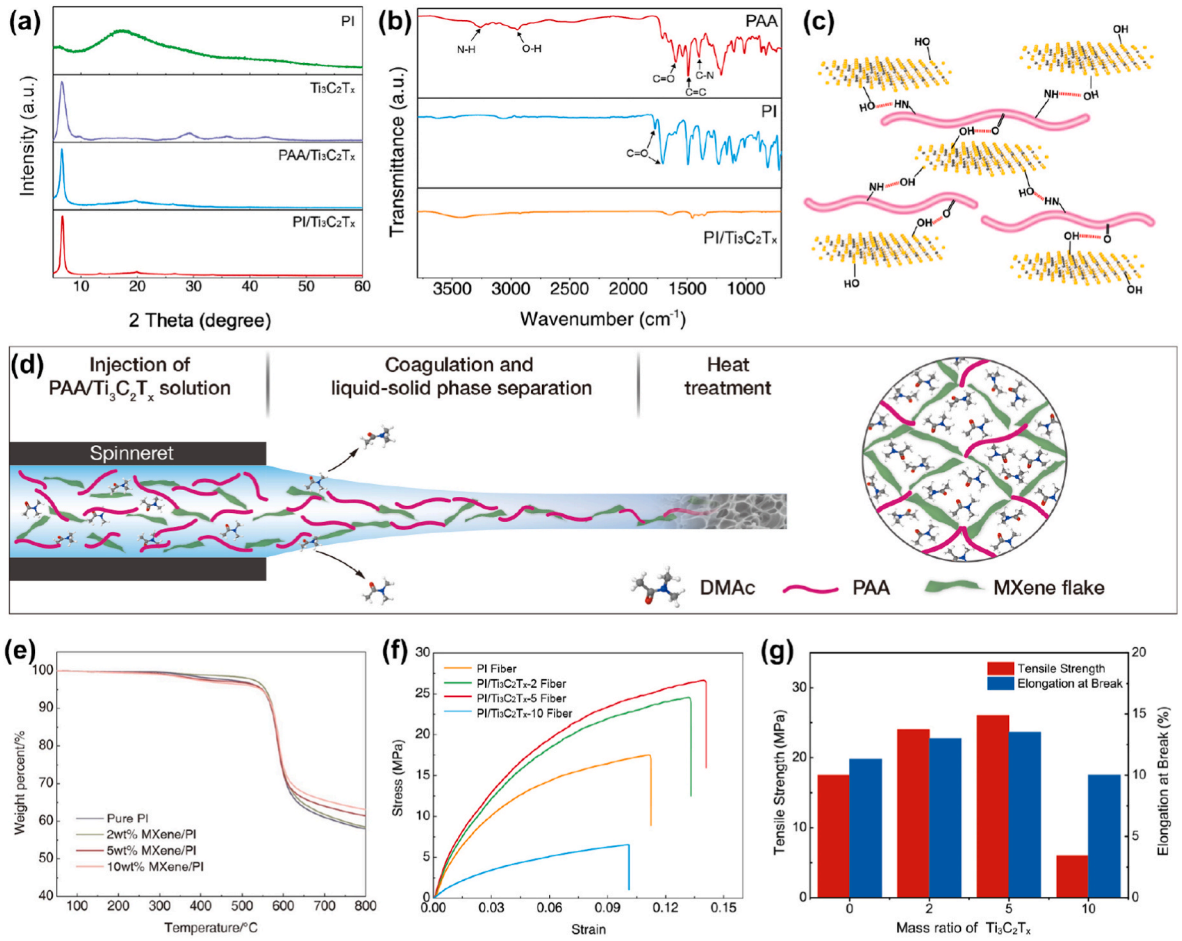

Fig. 3. (a, b) XRD patterns and FTIR spectra of different samples. (c) Illustration of the hydrogen bonding between PI and MXene. (d) The proposed mechanism for the formation of porosity in PI/$Ti_3C_2T_x$ aerogel fibers. (e) TGA curves of different fibers. (f, g) Mechanical properties of the wet-spun fibers.

aerogel fibers exhibit the highest residue weight due to the largest mass percentage of MXene. Apart from that, porous structures within the aerogel fibers can significantly improve the thermal stability because of the discontinuity of heat conduction. Mechanical strength is crucial for the practical applications of PI aerogel fibers and textiles. Therefore, tensile tests were performed on the aerogel fibers with different mass fractions of $Ti_3C_2T_x$ with results shown in Fig. 3(f) and (g). Excitingly, PI/$Ti_3C_2T_x$-2 and PI/$Ti_3C_2T_x$-5 aerogel fibers exhibit significantly increased tensile strength (24.0 MPa and 26.0 MPa) and elongation (13.0% and 13.5%) compared with pure PI fiber (17.5 MPa and 11.3%), which is possibly contributed by the intimate interfacial interaction between MXene flakes and PI macromolecular chains. However, when the mass fraction of $Ti_3C_2T_x$ rise to 10 wt%, the tensile strength and elongation decrease sharply to 6.0 MPa and 10%, respectively, this phenomenon is caused by the excessive filling content of $Ti_3C_2T_x$ flakes in the PI matrix, which may inhibit the necessary linking between PI chains. Considering the excellent porosity and the best mechanical properties of PI/$Ti_3C_2T_x$-5 threads, it is concluded that appropriate MXene incorporation is highly beneficial for the formation of robust PI-based aerogel fibers. As a result, the PI and PI/$Ti_3C_2T_x$ fibers can be easily weaved into flexible fabrics for diverse practical applications (Fig. S4). The digital photographs shown in Fig. S5 indicate the textiles woven by densely arranged fibers manifest excellent bendability without any damage.

Flame resistance is an essential property for the PI/$Ti_3C_2T_x$ aerogel fibers in many high-temperature applications, especially for protective clothing [30]. Hence, the ignition tests were performed on the PI fiber and different PI/$Ti_3C_2T_x$ aerogel fibers to compare their flame-resisting performance. As detailly listed in Fig. 4(a), neat PI fiber is ignited after contacting with the flame in a short time (in about 0.5 s), which keep burning with a length of about 5 mm even if the fire is moved away. Meanwhile, the PI/$Ti_3C_2T_x$-2 fiber and the PI/$Ti_3C_2T_x$-5 fiber also can be ignited but with a smaller flame, which self-extinguish instantly after the fire is withdrawn, implying the addition of MXene flakes in the PI matrix can largely improve the flame resistance capability of the aerogel fibers. It is also notable that the burning length of PI/$Ti_3C_2T_x$-5 aerogel fiber was significantly shorter than that of PI/$Ti_3C_2T_x$-2 fiber, which is highly correlated with the increased mass fraction of MXene in the PI matrix. As expected, the PI/$Ti_3C_2T_x$-10 fiber with the highest MXene incorporation is hard to ignite even after staying on the flame for 1 s. In a word, prepared PI/$Ti_3C_2T_x$ aerogel fibers manifest excellent flame resistance and rapid self-extinguishing performance derived from the hierarchical porous structures and the homogeneous hybridization of MXene flakes, which is highly desirable for practical applications in wearable protective clothing. Considering the abundant porosity inside the PI/$Ti_3C_2T_x$ aerogel fibers, it is expected that they may also possess excellent thermal insulation properties apart from the flame resistance capability. A series of infrared images of PI fiber and different PI/$Ti_3C_2T_x$ aerogel fibers were taken under varying temperatures from 25 to 250 °C on a hot stage. Fig. 4(b) provides two typical infrared images of different fibers at 80 and 230 °C. The temperature on the fiber surface is summarized in Fig. 4 (c). It is evident that the fiber with higher $Ti_3C_2T_x$ loading shows a lower surface temperature at the same stage temperature, the difference in thermal insulation is more remarkable at a higher stage temperature of 250 °C. Quantitatively, the thermal conductivities of different fiber samples were measured and plotted in Fig. 4(d), PI/$Ti_3C_2T_x$ aerogel fiber

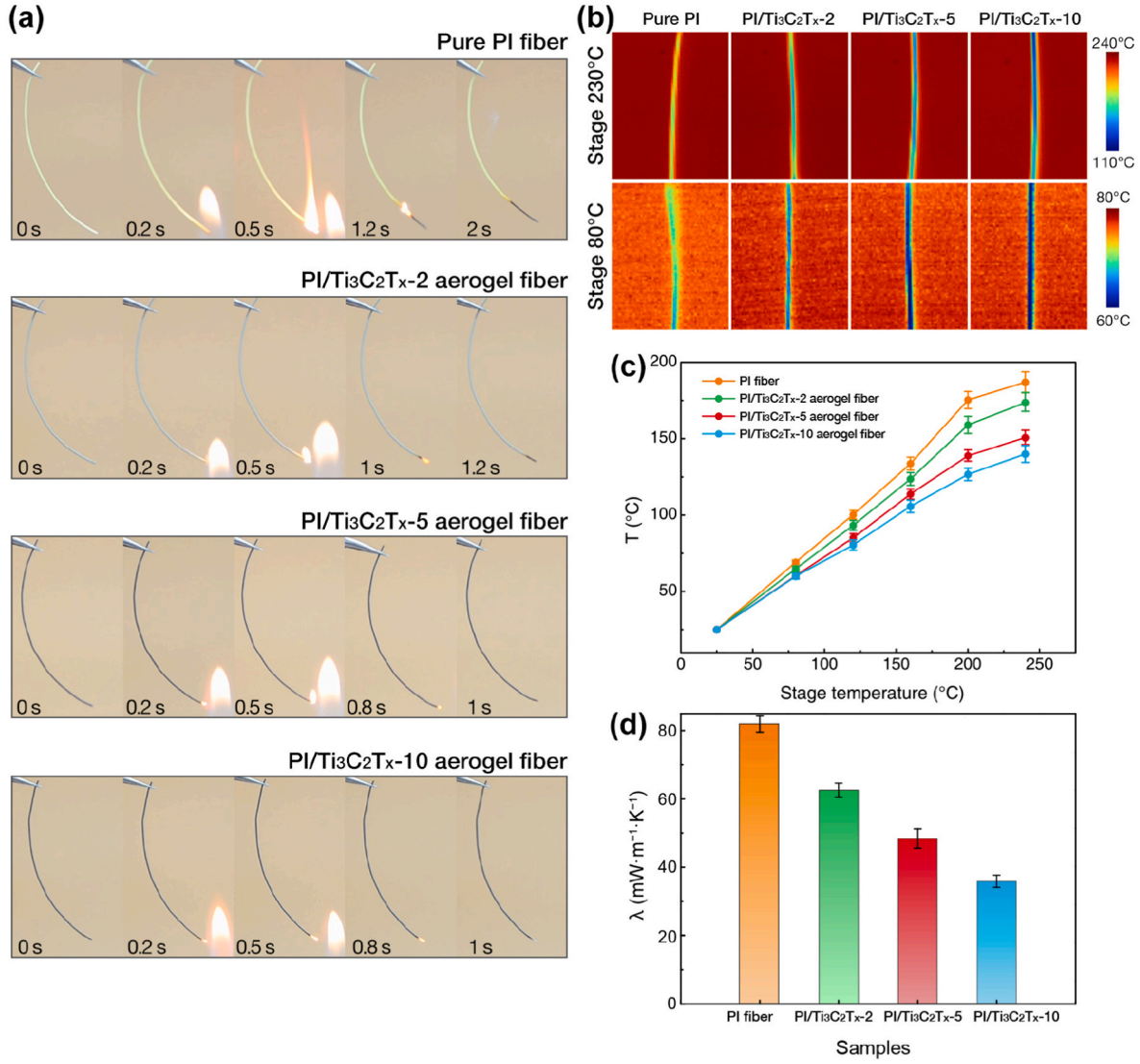

Fig. 4. (a) Ignition test comparison between different fibers (burning by an alcohol lamp, the maximum temperature is 700 °C). (b) Infrared images of different fibers on the hot stage with temperatures at 80 °C and 230 °C, and (c) the surface temperature plotted against the stage temperature. (d) The thermal conductivities of different fibers.

with 10 wt% MXene content shows a thermal conductivity as low as 36 mW m^{-1} K^{-1}, which is induced by the differentiated porosity caused by different MXene content, as we have discussed in Fig. 2. The excellent thermal insulation ability of the aerogel fibers is mainly contributed by their hierarchical pores, which could effectively reduce the heat conduction by trapping a large amount of air inside the voids.

To further investigate the practical applications of the aerogel fibers in protective textiles, pure PI and PI/$Ti_3C_2T_x$ textiles were weaved and placed on the same hot stage to compare their thermal insulating property. A series of infrared images were taken at different times under a constant stage temperature of 125 °C, three typical images at time points of 2 s, 10 s, and 30 s are shown in Fig. 5(a), and the surface temperatures of different textiles at varying times are plotted in Fig. 5 (b). As expected, textiles woven from the PI/$Ti_3C_2T_x$-10 aerogel fibers exhibit the best thermal insulation property with the slowest heating-up rate (55.4 °C after 30 s heating), which is definitely due to the smallest pores and largest surface area. By contrast, PI textiles show inferior thermal insulation with a surface temperature as high as 91.8°C after staying on the hot stage for 30 s. What is more, the surface temperature on each textile followed the declining trend with the $Ti_3C_2T_x$ loading, highlighting the importance of MXene flakes on the thermal insulation performance of wet-spun PI fibers and textiles. Fig. 5(c) schematically illustrates the heat transfer process inside the PI/$Ti_3C_2T_x$ aerogel fibers. In theory, the thermal conductivity is contributed by the thermal convection, the conductance of trapped air and PI matrix, and thermal radiation. The hierarchical porosity of the aerogel fibers could effectively restrict the air in isolated spaces, thus greatly inhibiting the thermal convection. Besides, the thermal conducting speed in highly porous fibers is significantly slower than that in solid one, and the abundant solid-air interface also effectively improve the reflectance of infrared light in the aerogel fibers, these factors function together to enhance the thermal insulation performance of prepared PI/$Ti_3C_2T_x$ aerogel fibers.

4. Conclusion

In summary, robust and uniform PI/$Ti_3C_2T_x$ aerogel fibers with hierarchical porosity were fabricated via in-situ polymerization and wet-spinning. Based on the intimate interfacial interaction between the monolayered $Ti_3C_2T_x$ flakes and the macromolecular chains, MXene was first homogeneously hybridized with polyamic acid through an in-situ polymerization method, which functions as the pore-generating agent to inhibit the phase separation of solvent in limited space through the

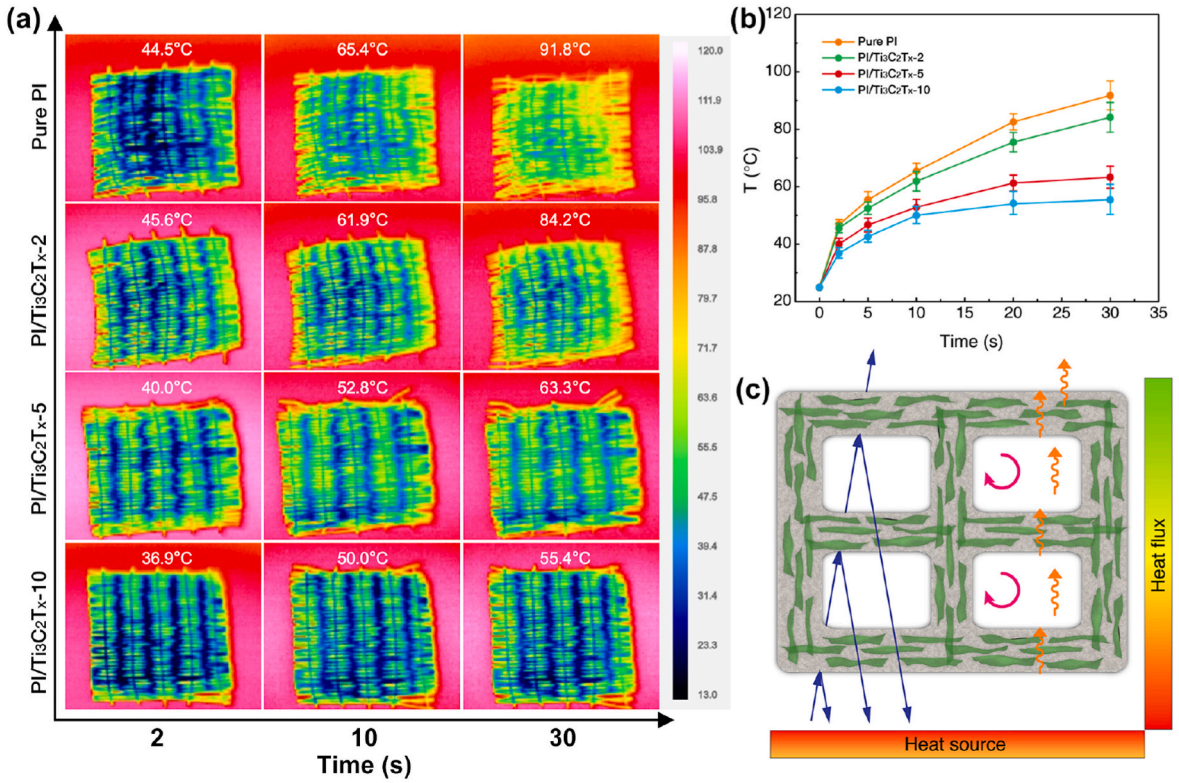

Fig. 5. (a) Infrared images of different textiles under a constant stage temperature of 125 °C, and (b) the surface temperature plotted against time. (c) Schematic illustration of the heat transfer in the aerogel fibers.

confinement of MXene networks, thus resulting in the multi-scaled porosity in the wet-spun PI/$Ti_3C_2T_x$ aerogel fibers. Consequently, the robust aerogel fibers showed largely improved mechanical properties (tensile strength of 26 MPa), high specific surface area (145 $m^2\ g^{-1}$), excellent flame resistance, and a low thermal conductivity of 36 mW $m^{-1}\ K^{-1}$, which can be easily fabricated into free-standing textiles for practical thermal regulation. Considering the scalability and functionality, this PI/$Ti_3C_2T_x$ aerogel fiber provides a promising candidate for next-generation thermal insulating textiles.

CRediT authorship contribution statement

Dan Wang: Methodology, Investigation, draft preparation. **Yidong Peng:** Investigation, Data curation. **Jiancheng Dong:** Investigation, Data curation. **Lei Pu:** Data curation, Validation. **Kangqi Chang:** Data curation, Validation. **Xiu-Ping Yan:** Writing – review & editing. **Hai-Long Qian:** Writing – review & editing. **Le Li:** Validation, Conceptualization, Writing – review & editing. **Yunpeng Huang:** Data curation, Validation, Supervision, Conceptualization, Writing – review & editing. **Tianxi Liu:** Conceptualization, Methodology, Supervision, Writing – review & editing.

Declaration of competing interest

The authors declare that they have no known competing financial interests or personal relationships that could have appeared to influence the work reported in this paper.

Data availability

The authors do not have permission to share data.

Acknowledgements

This work is financially supported by the National Natural Science Foundation of China (21875033), the China Postdoctoral Science Foundation (2022M711355), the Natural Science Foundation of Jiangsu Province (BK20221540), the Shanghai Scientific and Technological Innovation Project (18JC1410600), the Program of the Shanghai Academic Research Leader (17XD1400100), the State Key Laboratory for Modification of Chemical Fibers and Polymer Materials, Donghua University, and the Postgraduate Research & Practice Innovation Program of Jiangsu Province (KYCX22_2317).

Appendix A. Supplementary data

Supplementary data related to this article can be found at https://doi.org/10.1016/j.coco.2022.101429.

References

[1] Y. Peng, Y. Cui, Advanced textiles for personal thermal management and energy, Joule 4 (4) (2020) 724–742, https://doi.org/10.1016/j.joule.2020.02.011.
[2] G. Liu, Y. Xiong, L. Zhou, Additive manufacturing of continuous fiber reinforced polymer composites: design opportunities and novel applications, Compos. Commun. 27 (2021), 100907, https://doi.org/10.1016/j.coco.2021.100907.
[3] W. Fan, X. Zhang, Y. Zhang, Y.F. Zhang, T.X. Liu, Lightweight, strong, and super-thermal insulating polyimide composite aerogels under high temperature, Compos. Sci. Technol. 173 (2019) 47–52, https://doi.org/10.1016/j.compscitech.2019.01.025.
[4] J. Lyu, Z. Liu, X. Wu, G. Li, D. Fang, X. Zhang, Nanofibrous Kevlar aerogel films and their phase-change composites for highly efficient infrared stealth, ACS Nano 13 (2) (2019) 2236–2245, https://doi.org/10.1021/acsnano.8b08913.
[5] J. Tian, Y. Yang, T. Xue, G. Chao, W. Fan, T. Liu, Highly flexible and compressible polyimide/silica aerogels with integrated double network for thermal insulation and fire-retardancy, J. Mater. Sci. Technol. 105 (2022) 194–202, https://doi.org/10.1016/j.jmst.2021.07.030.
[6] Q. Zhang, T. Xue, J. Tian, Y. Yang, W. Fan, T. Liu, Polyimide/boron nitride composite aerogel fiber-based phase-changeable textile for intelligent personal

thermoregulation, Compos. Sci. Technol. 226 (2022), 109541, https://doi.org/10.1016/j.compscitech.2022.109541.
[7] F.G. Omenetto, D.L. Kaplan, New opportunities for an ancient material, Science 329 (5991) (2010) 528–531, https://doi.org/10.1126/science.1188936.
[8] S.W. Cranford, A. Tarakanova, N.M. Pugno, M.J. Buehler, Nonlinear material behaviour of spider silk yields robust webs, Nature 482 (7383) (2012) 72–76, https://doi.org/10.1038/nature10739.
[9] C.S. Fuller, C.J. Frosch, N.R. Pape, Chain structure of linear polyesters—trimethylene glycol series, J. Am. Chem. Soc. 64 (1) (1942) 154–160, https://doi.org/10.1021/ja01253a042.
[10] X. Zhang, Y. Liu, Y. Si, J. Yu, B. Ding, Flexible and tough zirconia-based nanofibrous membranes for thermal insulation, Compos. Commun. 33 (2022), 101219, https://doi.org/10.1016/j.coco.2022.101219.
[11] F. Hu, S. Wu, Y. Sun, Hollow-structured materials for thermal insulation, Adv. Mater. 31 (38) (2019), 1801001, https://doi.org/10.1002/adma.201801001.
[12] L. Raeisian, Z. Mansoori, R. Hosseini-Abardeh, R. Bagherzadeh, An investigation in structural parameters of needle-punched nonwoven fabrics on their thermal insulation property, Fibers Polym. 14 (10) (2013) 1748–1753, https://doi.org/10.1007/s12221-013-1748-1.
[13] W. Hu, X. Shi, M. Gao, C. Huang, T. Huang, N. Zhang, J. Yang, X. Qi, Y. Wang, Light-actuated shape memory and self-healing phase change composites supported by MXene/waterborne polyurethane aerogel for superior solar-thermal energy storage, Compos. Commun. 28 (2021), 100980, https://doi.org/10.1016/j.coco.2021.100980.
[14] M. He, M.K. Alam, H. Liu, M. Zheng, J. Zhao, L. Wang, L. Liu, X. Qin, J. Yu, Textile waste derived cellulose based composite aerogel for efficient solar steam generation, Compos. Commun. 28 (2021), 100936, https://doi.org/10.1016/j.coco.2021.100936.
[15] L. Pu, Y.P. Liu, L. Li, C. Zhang, P.M. Ma, W.F. Dong, Y.P. Huang, T.X. Liu, Polyimide nanofiber-reinforced Ti3C2Tx aerogel with "lamella-pillar" microporosity for high-performance piezoresistive strain sensing and electromagnetic wave absorption, ACS Appl. Mater. Interfaces 13 (2021) 47134–47146, https://doi.org/10.1021/acsami.1c13863.
[16] L. Pu, H. Ma, J. Dong, C. Zhang, F. Lai, G. He, P.M. Ma, W.F. Dong, Y.P. Huang, T. X. Liu, Xylem-Inspired polyimide/MXene aerogels with radial lamellar architectures for highly sensitive strain detection and efficient solar steam generation, Nano Lett. 22 (2022) 4560–4568, https://doi.org/10.1021/acs.nanolett.2c01486.
[17] M. Zhang, J. Yuan, Graphene meta-aerogels: when sculpture aesthetic meets 1D/2D composite materials, Nano Res. Energy 1 (2022), e9120035, https://doi.org/10.26599/NRE.2022.9120035.
[18] W. Zhang, M. Jiang, S. Yang, Y. Hu, B. Mu, Z. Tie, Z. Jin, In-situ grown CuOx nanowire forest on copper foam: a 3D hierarchical and freestanding electrocatalyst with enhanced carbonaceous product selectivity in CO2 reduction, Nano Res. Energy 1 (2022), e9120033, https://doi.org/10.26599/NRE.2022.9120033.
[19] Y. Wang, Y. Cui, Z. Shao, W. Gao, W. Fan, T.X. Liu, H. Bai, Multifunctional polyimide aerogel textile inspired by polar bear hair for thermoregulation in extreme environments, Chem. Eng. J. 390 (2020), 124623, https://doi.org/10.1016/j.cej.2020.124623.
[20] O.A. Tafreshi, S.G. Mosanenzadeh, S. Karamikamkar, Z. Saadatnia, C.B. Park, H. E. Naguib, A review on multifunctional aerogel fibers: processing, fabrication, functionalization, and applications, Mater, Today Chem 23 (2022), 100736, https://doi.org/10.1016/j.mtchem.2021.100736.
[21] X. Li, G. Dong, Z. Liu, X. Zhang, Polyimide aerogel fibers with superior flame resistance, strength, hydrophobicity, and flexibility made via a universal sol-gel confined transition strategy, ACS Nano 15 (3) (2021) 4759–4768, https://doi.org/10.1021/acsnano.0c09391.
[22] Y. Cui, H. Gong, Y. Wang, D. Li, H. Bai, A thermally insulating textile inspired by polar bear hair, Adv. Mater. 30 (14) (2018), e1706807, https://doi.org/10.1002/adma.201706807.
[23] Y. Guo, X. Yang, K. Ruan, J. Kong, M. Dong, J. Zhang, J. Gu, Z. Guo, Reduced graphene oxide heterostructured silver nanoparticles significantly enhanced thermal conductivities in hot-pressed electrospun polyimide nanocomposites, ACS Appl. Mater. Interfaces 11 (28) (2019) 25465–25473, https://doi.org/10.1021/acsami.9b10161.
[24] X. Wu, S. Shi, B. Tang, J. Chen, L. Shan, Y. Gao, Y. Wang, T. Jiang, K. Sun, K. Yang, J. Yu, Achieving highly thermal conductivity of polymer composites by adding hybrid silver–carbon fiber fillers, Compos. Commun. 31 (2022), 101129, https://doi.org/10.1016/j.coco.2022.101129.
[25] B. Shi, B. Ma, C. Wang, H. He, L. Qu, B. Xu, Y. Chen, Fabrication and applications of polyimide nano-aerogels, Composites, Part A 143 (2021), 106283, https://doi.org/10.1016/j.compositesa.2021.106283.
[26] S. Ghaffari-Mosanenzadeh, O. Aghababaei Tafreshi, S. Karamikamkar, Z. Saadatnia, E. Rad, M. Meysami, H.E. Naguib, Recent advances in tailoring and improving the properties of polyimide aerogels and their application, Adv. Colloid Interface Sci. 304 (2022), 102646, https://doi.org/10.1016/j.cis.2022.102646.
[27] O.A. Tafreshi, S. Ghaffari-Mosanenzadeh, S. Karamikamkar, Z. Saadatnia, S. Kiddell, C.B. Park, H.E. Naguib, Novel, flexible, and transparent thin film polyimide aerogels with enhanced thermal insulation and high service temperature, J. Mater. Chem. C 10 (13) (2022) 5088–5108, https://doi.org/10.1039/D1TC06122D.
[28] S. Meng, J. Zhang, W. Chen, X. Wang, M. Zhu, Construction of continuous hollow silica aerogel fibers with hierarchical pores and excellent adsorption performance, Microporous Mesoporous Mater. 273 (2019) 294–296, https://doi.org/10.1016/j.micromeso.2018.07.021.
[29] Y. Li, X.F. Liu, X.Y. Nie, W.W. Yang, Y.D. Wang, R.H. Yu, J.L. Shui, Multifunctional organic–inorganic hybrid aerogel for self-cleaning, heat-insulating, and highly efficient microwave absorbing material, Adv. Funct. Mater. 29 (10) (2019), 1807624, https://doi.org/10.1002/adfm.201807624.
[30] H. He, J. Liu, Y. Wang, Y. Zhao, Y. Qin, Z. Zhu, Z. Yu, J. Wang, An ultralight self-powered fire alarm e-textile based on conductive aerogel fiber with repeatable temperature monitoring performance used in firefighting clothing, ACS Nano 16 (2) (2022) 2953–2967, https://doi.org/10.1021/acsnano.1c10144.